International Journal of Engineering Inventions
e-ISSN: 2278-7461, p-ISSN: 2319-6491
Volume 12, Issue 7 [July. 2023] PP: 110-122

Development of Thermodynamic Equation of State for Normal Butane with Comprehensive Assessment

Koemleng Kan[1], I Made Astina[2,3]
[1] National Polytechnic Institute of Cambodia, Phum Prey Popel, SK. Somrong Krom, Khan Po Sen Chey, Phnom Penh, Cambodia.
[2] Faculty of Mechanical and Aerospace Engineering, Institut Teknologi Bandung, Jalan Ganesa 10, Bandung 40132, Indonesia.
[3] *Corresponding Author*

Abstract: *A new fundamental equation of state in the form of Helmholtz free energy function was developed to present thermodynamic properties of fluid phase normal butane. A genetic algorithm combined with weighted least square regression was applied to optimize the structural form and the numerical coefficients of the equation. The average absolute deviations are estimated to be 0.15% in liquid density, 0.32% in gaseous density, 0.037% in saturated-liquid density, 0.36% in saturated-vapor density except at higher temperature and triple point temperature, 0.31% in vapor pressure except at lower temperatures, 0.015% in ideal-gas isobaric specific heat, 0.39% in specific-heat capacity, 0.08% in speed of sound in gaseous phase, 0.53% in speed of sound in liquid phase. The equation of state is valid in the range of temperatures from triple point (134.87 K) to 700 K and pressures up to 300 MPa.*

Keywords: *thermodynamic, Helmholtz equation of state, normal butane, hydrocarbon, refrigerant.*

Date of Submission: 06-07-2023 Date of Acceptance: 19-07-2023

I. INTRODUCTION

In today's engineering interest, natural fluid like normal butane (R-600) and their mixtures have notable not only in the natural gas industry but also as key components in environmental working fluids of thermal engineering major. R-600 have no effect to the stratospheric ozone depletion and global warming. It has been widely used as a potential refrigerant for household air-conditioning system, refrigerants in domestic refrigerator-freezer, refrigerant of heat pump, refrigerant of chiller system, power gas in aerosols, fuel gas in liquefied, and used as a working fluid of thermal power plant. Concern on the above background, reliable and accurate equations of state for pure R-600 is needed for development of thermodynamic property models of mixtures.

EOS modeling in the Helmholtz free energy function is highly dependent on the experimental measurements used in its development. Several theoretical obstacles were encountered in the development to improve the consistency and reliability of the EOS. Extrapolation of PVT surface and caloric properties and ideal curves is assessed to reveal its behavior over a wide range from melting point to high temperatures and pressures. EOS which has reasonable behavior from the aspect of surface thermodynamics and an ideal curve is believed to be valid in all fluid phases even in a range of experimental data that is scarce or does not yet exist.

Equation of state (EOS) for R-600 has been developed in Helmholtz free energy by Chan et al. [1], Bücker and Wagner [2], Miyamoto and Watanabe [3], Span and Wagner [4], and Younglove and Ely [5] on the EOS MBWR. Chan et al. developed EOS for R-600 in a Helmholtz free energy function consisting of 18 terms for both fluids. The model is valid from temperature 135 K to 600 K and pressure to 69 MPa for R-600. Bücker and Wagner proposed the EOS consisting of 25 terms. The modeling includes melting points up to a temperature of 575 K and a pressure of 69 MPa. Ito et al. [6] reported experimental measurements of hydrocarbons, including R-600 for temperatures up to 600 K and pressures up to 200 MPa. Based on our assessment, most existing models fail to obtain a reasonable Joule inversion curve and have a higher deviation for calculating data at higher pressures up to 200 MPa.

The most reliable and accurate thermodynamic properties play significant role in finding prospective candidate working fluids for the interest of engineering. Accurate analysis result for thermal system design contributes to the improvements of system efficiency and results in energy saving. High performance of thermal systems with ozone friendly and negligible global warming potential substances are expected to improve the global environmental issue. Therefore, it is very important to develop reliable Helmholtz EOS for R-600.

Development method was firstly applied for difluoromethane (R-32) and reported in a previous paper [7]. More detailed procedure and mathematical relations of the development can be found in a reference [8].

II. DATA PREPARATION AND MODELING PROCEDURE

As an important part of the study, experimental measurements such as *pressure-volume-temperature* (*PVT*) in single-phase region, isobaric and isochoric specific heats, saturated heat capacity, saturation property measurements including Maxwell criteria, second and third virial coefficients, and speed of sound were selected as the input data for the model development. An accuracy of the input data for the modeling process contributes on the data reproducibility of the equation. All data with temperature standard older than ITS-90 were converted into ITS-90. In 2015, Herrmann and Vogel [9] published 294 of their *PVT* data in liquid phase. Ito et al. [6] reported 66 points of *PVT* data in liquid phase. Miyamoto and Uematsu [10] established 58 of *PVT* data point in compressed liquid phase. Glos et al. [11] reported 66 points of *PVT* data in accordance with data at saturation region including 22 points of vapour pressure, 9 points of saturated vapour-density, and 22 points of saturated-liquid density. All data used in the model of Chan et al. [1] and Miyamoto and Watanabe [12] are adopted in this study. The distribution of all experimental input data is shown in the Figure 1.

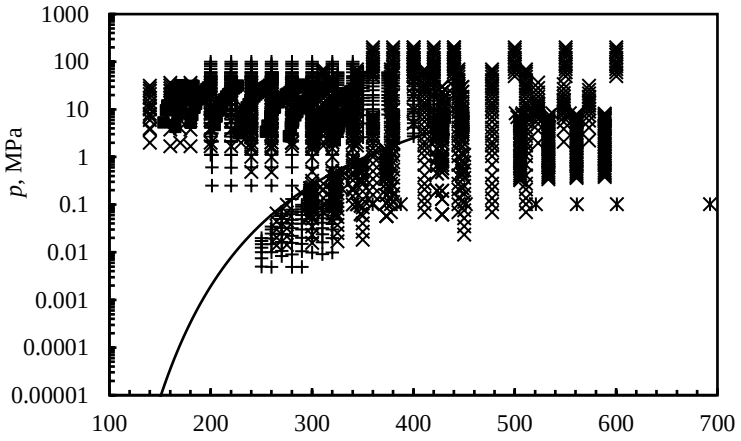

Figure 1. Experimental input data distribution for R-600. (×) *PVT*; (■) c_v; (∗) c_p; (+) w.

The critical parameters such as temperature (T_c=425.125 K, density (ρ_c=227.84 kg/m^3), pressure (p_c = 3.796 MPa) were selected from Haynes and Goodwin [13]. The adopted property from Chan et al. [1] is molar mass (M = 0.0581222 kg/mol). The triple point temperature (T_t = 134.895 K) was reported from Glos et al. [11]. The universal gas constant used is R = 8.3144598 [14]. Thermodynamic modelling of properties for R-600 was established in accordance with a convention recommended by International Institute of Refrigeration i.e., the references state of thermodynamic properties of specific entropy and enthalpy at the saturated liquid of 273.15 K with specific entropy of 1.0 kJ/kg·K and specific enthalpy of 200 kJ/kg.

In the development of this EOS, three steps must be conducted. The first step is to construct ancillary equations, which consist of the equation for saturated vapor pressure, saturated liquid density, and saturated vapor density equation. The three equations play a role in assisting the preparation of pressure-volume temperature of saturation line data and the implementation of the EOS that has been established. These equations have functions of temperature only. The second step is to develop the isobaric-specific heat equation for an ideal gas. This equation is also a function of temperature only. This equation plays a role in obtaining the ideal part of the EOS. The third step is to develop a residual part of the EOS.

Genetic algorithms have been widely applied in various engineering and science fields due to their effective power to get an optimal solution. In this modeling, the genetic algorithm combined with weighted least squares regression is applied to obtain additional equations and optimal EOS from the input data provided by minimizing the sum of the squared deviations from the data groups that have been prepared in modeling. This optimization procedure was originally developed and discussed in detail in previous work [8] and presented in our previous paper [15]. This optimization procedure was written in the program code C++ and applied to various refrigerants such as HFCs, hydrocarbons, and HFO. In principly, the nonlinear constants in the equation are generated from the genetic algorithm, while the related coefficients that have a linear relationship with the dependent variable are calculated from weighted least squares regression.

III. RESULTS AND ASSESSMENTS

3.1 Saturation Equations

Vapour pressure (p_s), saturated vapour density (ρ''), and saturated liquid density (ρ') of ancillary equations were developed and used in development of the Helmholtz equation of state. Modelling of the equations were conducted by fitting to each property input data. The mathematical models of p_s, ρ'', and ρ' are written in Equations (1), (2), and (3), respectively. Numerical coefficients and constants of the equations are listed in the Table 1.

$$\ln\left(\frac{p_s}{p_c}\right) = \sum_{i=1}^{3} A_i \frac{T_c}{T}\left(1-\frac{T}{T_c}\right)^{a_i} \tag{1}$$

$$\ln\left(\frac{\rho''}{\rho}\right) = \sum_{i=1}^{5} B_i \left(1-\frac{T}{T_c}\right)^{b_i} \tag{2}$$

$$\left(\frac{\rho'}{\rho}-1\right) = \sum_{i=1}^{6} C_i \left(1-\frac{T}{T_c}\right)^{c_i} \tag{3}$$

Table 1. Numerical coefficients and power constants of the equations

	Eq. (1)		Eq. (2)		Eq. (3)	
i	a_i	A_i	b_i	B_i	c_i	C_i
1	1.1	-18.1084	0.100	-0.151619	0.150	4.20112
2	1.2	12.4299	0.53575	-4.54497	0.250	-15.4277
3	3.5	-3.36864	2.0250	-11.8402	0.400	37.3879
4	-	-	5.000	-31.6141	0.51667	-37.3092
5	-	-	9.375	-61.1207	0.641667	13.7641
6	-	-	-	-	3.89167	0.201793

3.2 New Thermodynamic Equation of State

The new equation of state expressed in the function of Helmholtz free energy is divided into two parts, which consist of ideal part (α^0) and residual part (α^r). The ideal part is state for the ideal characteristic of fluid, which consists of eight terms for present model. The residual part consisting of 17 terms identifies the difference between a real property and an ideal gas property, both considered at the same pressure, temperature, and composition. The ideal part was obtained from the ideal gas isobaric specific heat equation by applying the integration process along with the reference state values. Ideal gas isobaric specific heat, ideal part, and residual part are given in Equations (4), (5), and (6), respectively. This EOS has a structural form as a result of simultaneous optimization as introduced in previous paper [16]. All thermodynamic properties can be derived using relations listed in Table 2. The numerical coefficients and power constants of Equations (4) (5), and (6) are listed in the Tables 3 and 4. In each correlation thermodynamic property $\tau = T_c/T$ and $\delta = \rho/\rho_c$ as independent parameters of Equations (5) and (6) are given in Table 2.

$$\frac{c_p^0}{R} = 1 + N_1^0 + \sum_{i=2}^{6} N_i^0 \eta_i^{0^2} \tau^2 \frac{\exp(\eta_i^0 \tau)}{\left[1-\exp(\eta_i^0 \tau)\right]^2} \tag{4}$$

$$\alpha^0(\delta,\tau) = \ln\tau + N_1^0 + N_2^0\tau + N_3^0 \ln\tau + \sum_{i=4}^{8} N_i^0 \ln[1-\exp(-\eta_i^0\tau)] \tag{5}$$

$$\alpha^r(\delta,\tau) = \sum_{i=1}^{11} N_i \delta^{d_i}\tau^{t_i} + \sum_{i=12}^{13} N_i \delta^{d_i}\tau^{t_i}\exp[-\delta] + \sum_{i=14}^{14} N_i \delta^{d_i}\tau^{t_i}\exp[-\delta^2] + \sum_{i=15}^{17} N_i \delta^{d_i}\tau^{t_i}\exp[-\delta^3] \tag{6}$$

Table 2. Thermodynamic properties derived from EOS.

Property	Thermodynamic property relations
Saturated vapor pressure	$\frac{p_s(\delta',\delta'',\tau_s)}{RT_s} = \frac{\rho'\rho''}{\rho'-\rho''}\left(\ln\left(\frac{\delta'}{\delta''}\right) + \alpha^{r\prime} - \alpha^{r\prime\prime}\right)$
Pressure	$\frac{p(\delta,\tau)}{\rho RT} = 1 + \delta\alpha_\delta^r$
Isobaric specific heat	$\frac{c_p(\delta,\tau)}{R} = \frac{c_v(\delta,\tau)}{R} + \frac{(1+\delta\alpha_\delta^r - \delta\tau\alpha_{\delta\tau}^r)^2}{(1+2\delta\alpha_\delta^r + \delta^2\alpha_{\delta\delta}^r)}$
Isochoric specific heat	$c_v(\delta,\tau)/R = -\tau^2(\alpha_{\tau\tau}^0 + \alpha_{\tau\tau}^r)$
Speed of Sound	$\frac{w^2(\delta,\tau)M}{RT} = 1 + 2\delta\alpha_\delta^r + \delta^2\alpha_{\delta\delta}^r + \frac{(1+\delta\alpha_\delta^r - \delta\tau\alpha_{\delta\tau}^r)^2}{c_v(\delta,\tau)/R}$

Property	Thermodynamic property relations
Saturated liquid specific heat	$\frac{{c_s}'(\delta',\delta'',\tau_s)}{R}=\frac{c_v(\delta',\tau_s)}{R}+\frac{\left(1+\delta'\alpha_\delta^{r\prime}-\delta'\tau_s\alpha_{\delta\tau}^{r\prime}\right)}{\left(1+2\delta'\alpha_\delta^{r\prime}+\delta'^2\alpha_{\delta\delta}^{r\prime}\right)}\times\left\{1+\delta'\alpha_\delta^{r\prime}-\delta'\tau_s{\alpha_{\delta\tau}^r}'-\frac{1}{R\rho_c\delta'}\frac{dp_s(\delta',\delta'',\tau_s)}{dT}\right\}$
Saturated vapor specific heat	$\frac{{c_s}''(\delta',\delta'',\tau_s)}{R}=\frac{c_v(\delta'',\tau_s)}{R}+\frac{(1+\delta''\alpha_\delta^{r\prime}-\delta''\tau_s\alpha_{\delta\tau}^{r\prime\prime})}{(1+2\delta''\alpha_\delta^{r\prime\prime}+\delta''^2\alpha_{\delta\delta}^{r\prime\prime})}\times\left\{1+\delta''\alpha_\delta^{r\prime\prime}-\delta''\tau_s\alpha_{\delta\tau}^{r\prime\prime}-\frac{1}{R\rho_c\delta''}\frac{dp_s(\delta',\delta'',\tau_s)}{dT}\right\}$
Internal energy	$\frac{u(\delta,\tau)}{RT}=\tau(\alpha_\tau^0+\alpha_\tau^r)$
Enthalpy	$\frac{h(\delta,\tau)}{RT}=\tau(\alpha_\tau^0+\alpha_\tau^r)+1+\delta\alpha_\delta^r$
Entropy	$\frac{s(\delta,\tau)}{R}=\tau(\alpha_\tau^0+\alpha_\tau^r)-(\alpha^0+\alpha^r)$
Ideal-gas isobaric-specific heat	$\frac{c_p^0}{R}=1-\tau^2\alpha_{\tau\tau}^0=1+\frac{c_v^0(\tau)}{R}$
Second virial coefficient	$B(\tau)\rho_c=\lim_{\delta\to0}\alpha_\delta^r$
Third virial coefficient	$C(\tau)\rho_c^2=\lim_{\delta\to0}\alpha_{\delta\delta}^r$
	$\alpha_\delta=\left(\frac{\partial\alpha}{\partial\delta}\right)_\tau,\ \alpha_{\delta\delta}=\left(\frac{\partial^2\alpha}{\partial\delta^2}\right)_\tau,\ \alpha_\tau=\left(\frac{\partial\alpha}{\partial\tau}\right)_\delta,\ \alpha_{\tau\tau}=\left(\frac{\partial^2\alpha}{\partial\tau^2}\right)_\delta,\ \alpha_{\delta\tau}=\left(\frac{\partial^2\alpha}{\partial\delta\partial\tau}\right),\ \delta=\frac{\rho}{\rho_c},\ \tau=\frac{T_c}{T}$

Table 3. Numerical and functional form of ideal part

i	η_i^0	N_i^0
1	-	-5.4724193
2	-	4.9149033
3	-	3.280838
4	9.719619	10.37331
5	4.145391	14.61794
6	2.540154	4.325808
7	1.340637	-1.38211
8	0.811438	6.24926

Table 4. Numerical and functional form of residual part

i	d_i	t_i	N_i
1	3	0.75	5.9311430×10^{-02}
2	4	1.95	7.6128732×10^{-03}
3	1	0.26	$1.3051076\times10^{+00}$
4	1	1.2	$-7.8458715\times10^{+00}$
5	1	1.34	$5.7492978\times10^{+00}$
6	2	0.26	1.7044398×10^{-01}
7	2	1.34	-1.5888725×10^{-01}
8	3	1.77	-7.3942328×10^{-02}
9	4	0.46	3.17067227×10^{-03}
10	6	0.47	8.7012511×10^{-04}
11	6	1.38	4.7333397×10^{-04}
12	1	2.75	-3.5863945×10^{-01}
13	1	3.25	9.2066535×10^{-02}
14	1	4.225	-1.8207233×10^{-01}
15	4	4	-5.5743324×10^{-02}
16	9	8	-1.2560357×10^{-03}
17	2	8	-3.2303278×10^{-02}

3.3 Assessment and Discussion

The assessments of the new EOS resulted from this study are important to reveal its reliability and accuracy. The first criteria that confirm the accuracy of the EOS is their ability to reproduce the accurate experimental data with a minimum deviation. Experimental data were compared to the data calculated from the new EOS at the same given condition. The deviation referred to in the analysis is the relative value expressed in percent, which is a comparison of the property value obtained from the EOS of this work with experimental data or other existing equations

The new EOS can be accurately reproduced the c_p^0 data of Chen et al. [17] with deviation of 0.06% as plotted in Figure 2. Deviations of existing models such as Chan et al. [1], Miyamoto and Watanabe [12], and

Jaecke and Schley [18] are reliable represented to the data of Chen et al. [17] within the range of validity from temperatures 50 K to 1500 K.

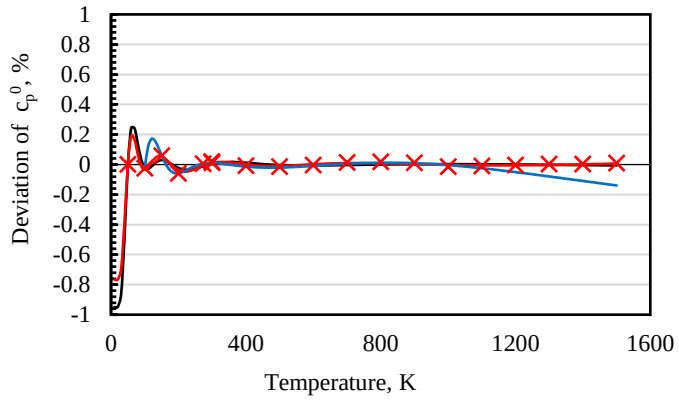

Figure 2. Deviation of ideal-gas isobaric specific heat equation for R-600. (×) Chen et al. [17]; (——) Chan et al. [1]; (——) Miyamoto and Watanabe [12] ; (——) Jaecke and Schley [18].

Figure 3 shows the deviations of liquid density calculated from the new EOS for R-600. Deviations of liquid densities from different sources are mostly represented within ±0.25% from lower to higher temperatures. The data of Herrmann and Vogel [9], Ito et al. [6], Miyamoto and Uematsu [10], Kayukawa et al. [19], Glos et al. [11], Olds et al. [20], and Haynes [21] are accurately reproduced with average absolute deviations (AAD) 0.17%, 0.20%, 0.15%, 0.14%, 0.04%, 0.27%, and 0.05%, respectively. Two data points of Ito et al. reach maximal deviation higher than 0.5%. The single data point of Miyamoto and Uematsu and some data points of Herrmann and Vogel also have deviation bigger than 0.5%.

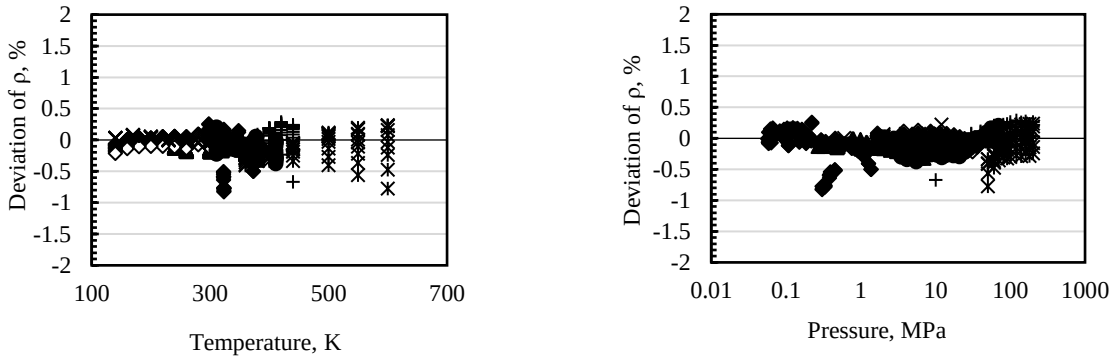

Figure 3. Deviations of liquid density from the new EOS for R-600 in liquid phase. (♦) Herrmann and Vogel [9]; (∗) Ito et al. [6]; (+) Miyamoto and Uematsu [10]; (×) Glos et al. [11]; (▲) Kayukawa et al. [19]; (●) Olds et al. [20]; (◊) Haynes [21].

Figure 4 indicates the deviations of experimental density data from the new EOS in gaseous phase. Most of input data can be represented with deviations within ±0.5%, except some data at higher temperatures. The data of Gupta and Eubank [22] are in good agreement with the new EOS along with AAD 0.03%. The data of Glos et al. [11] are accuracy represented with AAD 0.03%, except three data points which seem to be unreliable. The experimental data of Olds et al. [20] which exist over wider range of temperature have value of AAD equal to 0.27%. The measurement data of Kay [23] can be reproduced with AAD equal to 0.44%. Most of data calculated from the new EOS have good deviations in comparison to the existing EOSs.

Figure 5 shows illustrates the pressure deviations in gaseous phase from the present model. The data input of PVT property can be presented with deviations lower than ±1%, except 4 data points of Kay [23] have deviations higher than 1%.

The new EOS also covers for thermodynamic properties at saturation boundary. The assessment of PVT property at saturation phase including vapour-pressure, saturated-liquid density, and saturated-vapour density are necessary to reveal its accuracy. The data calculated from ancillary equations were also used in development of the EOS. The deviations of saturated-liquid density calculated from the new EOS are illustrated in Figure 6. As shown in the figure, most of saturated-liquid densities experimental input data including data of Glos et al.

[11], Orrit and Laupretre [24], Haynes and Hiza [25], McClune [26], Sliwinski [27], Olds et al. [20], and Magee and Lüddecke [28] can be accurately reproduced within ±0.25% from lower temperature to higher temperature. The deviations of data calculated from the existing EOSs of Chan et al. [1], Miyamoto and Watanabe [12], and Younglove and Ely [29] are plotted in the Figure 6.

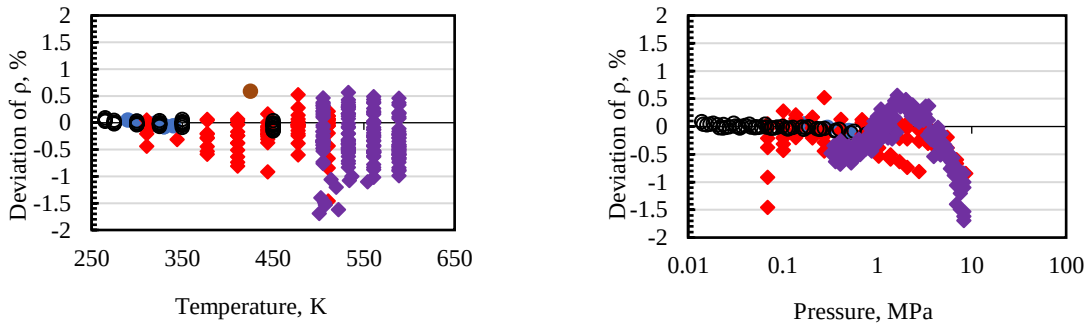

Figure 4. Deviation of gaseous density from the new EOS for R-600. (●) Glos et al. [11]; (♦) Olds et al. [20]; (○) Gupta and Eubank [22]; (♦) Kay [23].

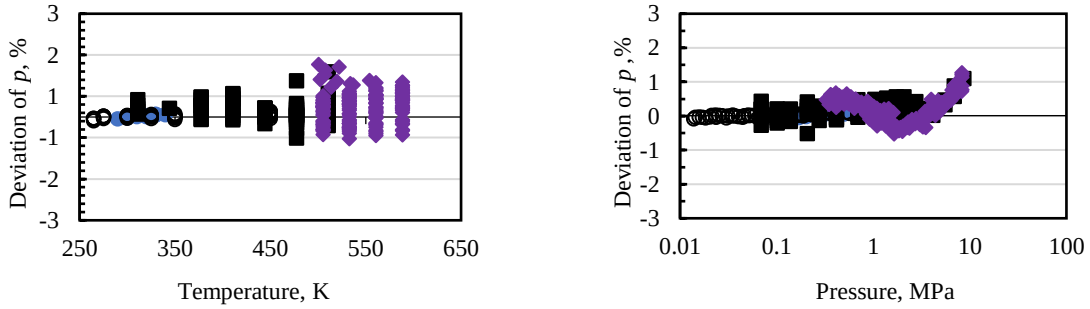

Figure 5. Deviations of pressures from the new EOS for R-600 in gaseous phase. (●) Glos et al. [11]; (■) Olds et al. [20]; (○) Gupta and Eubank [22]; (♦) Kay [23].

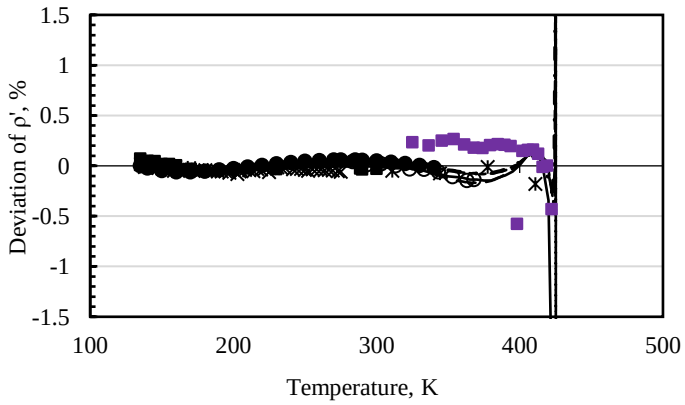

Figure 6. Deviation of saturated-liquid density data from the new EOS for R-600. (●) Glos et al. [11]; (×) Orrit and Laupretre [24]; (■) Haynes and Hiza [25]; (+) McClune [26]; (○) Sliwinski [27]; (∗) Olds et al. [20]; (-) Magee and Lüddecke [28]; (■) Kay [23]; (– - –) Ancillary Equation; (….) Chan et al. [1]; (---) Miyamoto and Watanabe [12]; (——) Young love and Ely [29].

Figure 7 shows the deviations of vapour-pressure calculated from the new EOS. The experimental data of Glos et al. [11] are better represented with deviations within ±0.5% for the range of temperatures from 140 K to 340 K. Most of input data can be reproduced with deviations within ±0.5% from temperature range from 210 K to 425.125 K, except some data of Machin and Golding [30] and Kay [23]. Vapor pressures at low temperatures have lower accurate reproduction of experimental data especially near the triple point. The deviations of existing

EOSs of Chan et al. [1], Miyamoto and Watanabe [12], Younglove and Ely [29] are also plotted. Most of all experimental input data can be better to be represented in comparison to the previous EOSs.

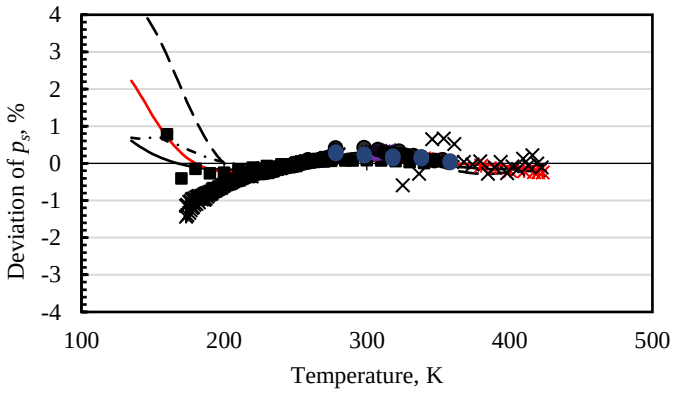

Figure 7. Deviations of vapor-pressure data from the new EOS for R-600. (■) Glos et al. [11]; (●) Holldorff and Knapp [31]; (∗) Kratzke et al. [32]; (×) Sako et al. [33]; (∗) Machin and Golding [30]; (●) Flebbe et al. [34]; (×) Kay [23]; (——) Ancillary Equation; (——) Chan et al. [1]; (----) Miyamoto and Watanabe [12]; (– - –) Younglove and Ely [29].

Figure 8 shows the deviations of saturated-vapor density from the new EOS. Experimental data of Glos et al. [11] which exist over the range of 220 K up to 340 K are in good agreement with deviation within ±0.1%. The other sets of data of Sliwinski [27] can be represented within ±0.04% and some data have deviations higher than 0.5%. The data of Olds et al. [20] have deviations within ±0.2 %, except one data point has deviation higher than 1%. The derived data of Chan et al. [1], Miyamoto and Watanabe [12], and Younglove and Ely [29] at higher and lower temperatures have lower accuracy.

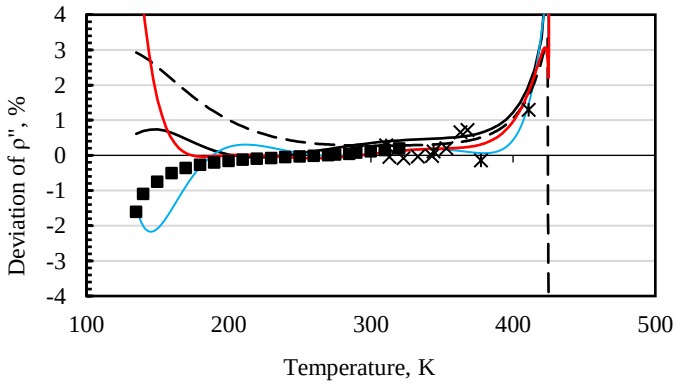

Figure 8. Deviation of saturated-vapor density data from the new EOS for R-600. (■) Glos et al. [11]; (×) Sliwinski [27]; (∗) Olds et al. [20]; (——) Ancillary Equation; (——) Chan et al. [1]; (----) Miyamoto and Watanabe [12]; (——) Younglove and Ely [29].

The isochoric specific heat c_v data in liquid phase of Magee and Lüddecke [28] are represented within ±1.5%. The deviations of liquid isochoric specific heat are plotted in Figure 9.

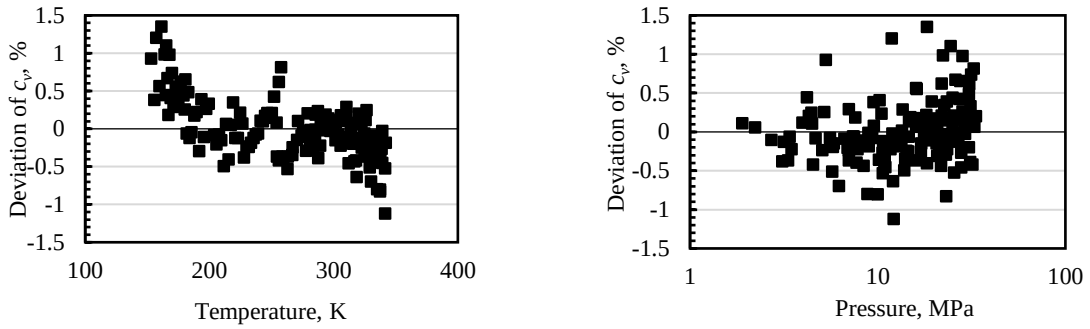

Figure 9. Deviation of isochoric specific heat in liquid phase from the new EOS for R-600. (■) Magee and Lüddecke [28].

Figure 10 shows the deviations of isobaric specific heat c_p in vapor phase. The isobaric specific heat data in gaseous phase of Dailey and Felsing [35] can be reproduced within deviations less than 0.5%, which corresponding to the AAD equal to 0.29%. The data of saturated liquid specific heat c_s of Magee and Lüddecke [28] can be reproduced with deviations within ±1% in the temperatures range 155 K to 316 K, except some data at low temperatures. The deviations of saturated liquid specific heat are plotted in Figure 11.

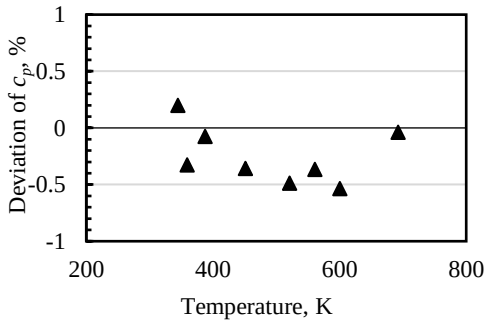

Figure 10. Deviation of isobaric specific heat from the new EOS for R-600. (▲) Dailey and Felsing [35].

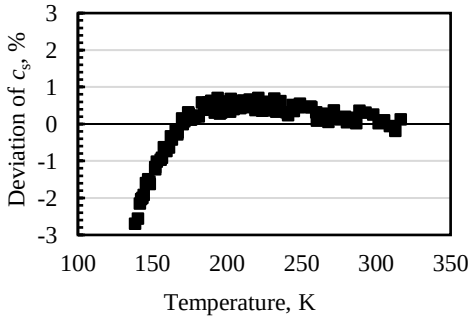

Figure 11. Deviation of saturated-liquid specific heat from the new EOS for R-600. (■) Magee and Lüddecke [28].

For acoustic property assessment, speed-of-sound data are assessed by visualizing in Figures 12 and 13. As shown in Figure 12, the deviation of speed-of-sound data in gaseous phase of Ewing et al. [36] are in good agreement with deviations within ±0.09%, which is corresponding to the AAD equal to 0.08%. In liquid phase, larger deviations can be observed in Figure 13. The speed of sound data in liquid phase of Hawary and Meier [37] and Niepmann [38] are generally represented with deviations within ±2%, except some data have deviation higher than 2%. The estimated AAD are 0.63%, and 0.36% for the data of Hawary and Meier, and Niepmann, respectively.

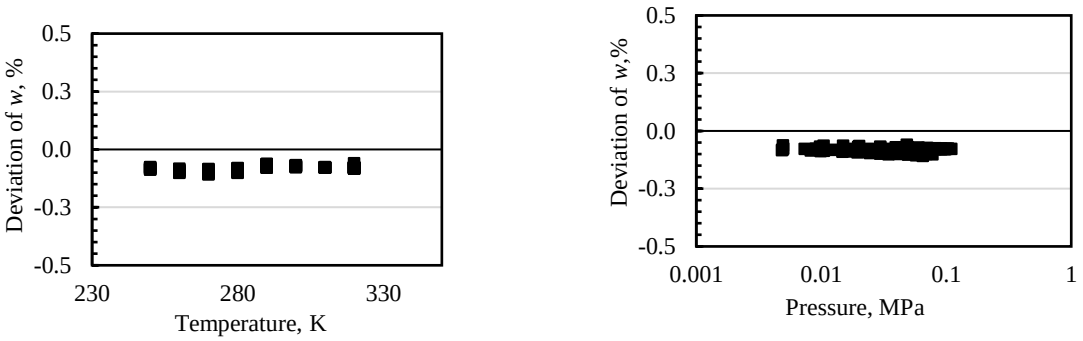

Figure 12. Deviation of speed-of-sound data in gaseous phase from the new EOS for R-600. (■) Ewing et al. [36].

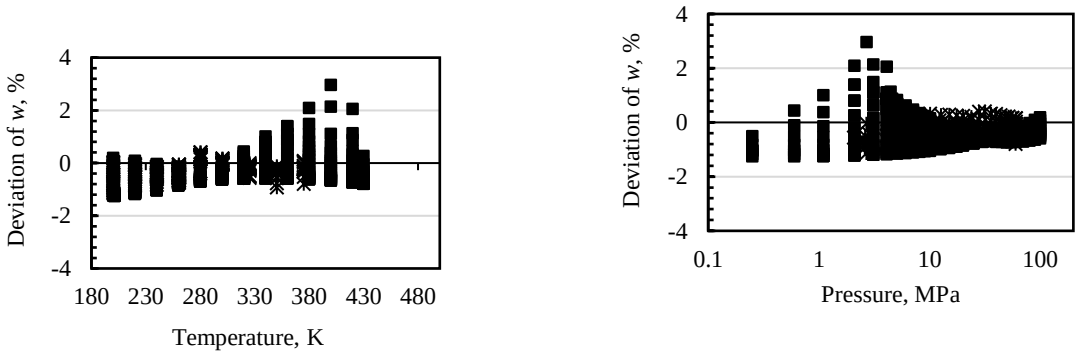

Figure 13. Deviation of speed-of-sound data in liquid phase from the new EOS for R-600. (■) Hawary and Meier [37]; (∗) Niepmann [38].

3.4 Extrapolation Behaviors of New Equation of State

An accuracy of thermodynamic EOS does not only depend on the uncertainties, but also the extrapolation behaviours which have significantly influenced in the modelling capacity. The smooth behaviours of caloric properties, isothermal lines of PVT, and acoustic property over the region where experimental data are not available are plotted in Figure 14.

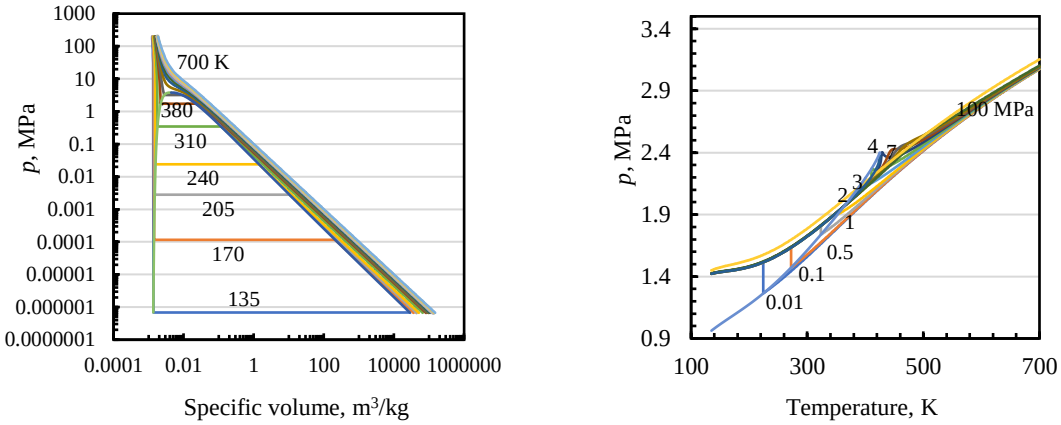

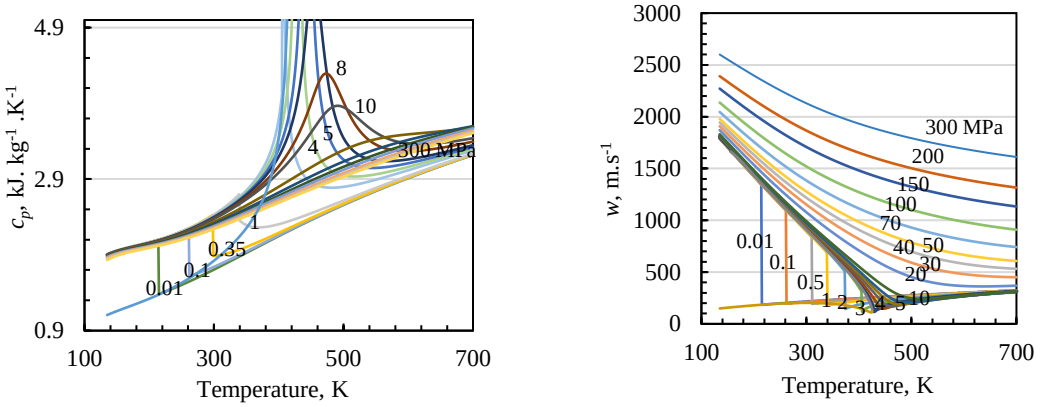

Figure 14. Extrapolation behaviors of PVT, c_p, c_p, and w from the new EOS

Investigating the behavior of second and third virial coefficients from the new EOS is an important criterion to confirm its presentation in accordance with an intermolecular potential theory. The smooth behaviour of second and third virial coefficients is illustrated in Figure 15. As one of another importance tests for the reliability and accuracy of EOS for R-600, reasonable ideal curves including Joule inversion, Joule-Thomson, and Boyle curves are shown in Figure 16. Since the ideal curves in this study are smoothly represented, therefore the selection of the structural form for the new EOS is closely related to the behavior of its ideal curve.

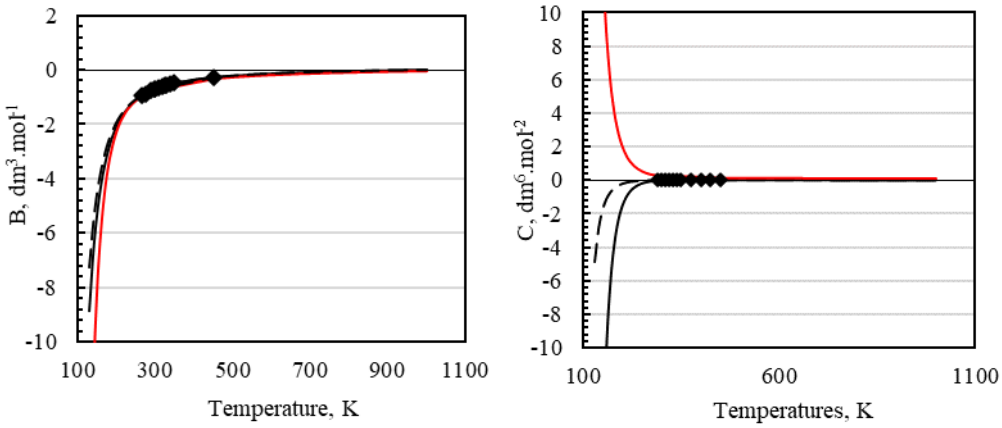

Figure 15. Second and third coefficients behavior derived from the new EOS for R-600. (♦) Glos et al. [11]; (——) This Study; (---) Chan et al. [1]; (——) Miyamoto and Watanabe [12].

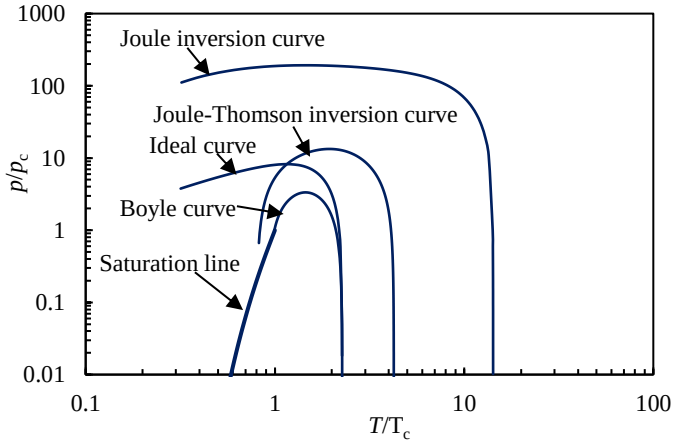

Figure 16. Ideal curves derived from the new EOS for R-600.

IV. CONCLUSION

Helmholtz EOS expressed in the function of reduced density and temperature was developed for R-600 along with intermolecular potential theory. The new EOS is valid from triple point temperature (T_t= 134.895 K) up to 700 K, which is corresponding to pressure 300 MPa. The AAD were evaluated to be 0.15% in liquid density, 0.32% in the gaseous density, 0.037% in the saturated-liquid density, 0.36% in the saturated-vapor density except at higher temperature and the triple point temperature, 0.31% in the vapor pressure except at lower temperatures, 0.015% in the ideal-gas isobaric specific heat, 0.39% in the heat capacities, 0.08% in speed of sound for the gaseous phase, 0.53% in speed of sound for the liquid phase.

Conflict of interest

There is no conflict to disclose.

ACKNOWLEDGEMENT

The authors are grateful to AUN/SEED-net program (ASEAN University Network/Southeast Asia Engineering Education Development Network) for financial support on the research.

Nomenclature

M	molar mass	[kg·mol^{-1}]
p	pressure	[MPa]
B	second virial coefficient	[dm^3·mol^{-1}]
c	specific heat	[kJ·kg^{-1}·K^{-1}]
w	speed of sound	[m·s^{-1}]
T	temperature	[K]
C	third virial coefficient	[dm^6·mol^{-2}]
R	universal gas constant,	[J. mol^{-1}. K^{-1}]
ρ	density	[kg·m^{-3}]
τ	inverse reduced temperature $\left(\frac{T_c}{T}\right)$	
α	reduced Helmholtz free energy	
δ	reduced density $\left(\frac{\rho}{\rho_c}\right)$	

Subscripts

c	critical parameter
p	process at constant pressure
v	process at constant volume
t	triple point
s	saturation

Superscripts

o	ideal part–
r	residual part
‘	saturated-liquid state
“	saturated-vapor state

REFERENCES

[1] S. Chan, I. M. Astina, P. S. Darmanto and H. Sato, "Thermodynamic Property Model of Wide-Fluid Phase N-Butane," *Jurnal Teknik Mesin*, vol. 22, no. 2, p. 44–54, 2007.

[2] D. Bücker and W. Wagner, "Reference Equations of State for the Thermodynamic Properties of Fluid Phase n-Butane and Isobutane," *Journal of Physical and Chemical Reference Data*, vol. 35, no. 2, p. 929–1019, 2006.

[3] H. Miyamoto and K. Watanabe , "Thermodynamic Property Model for Fluid-Phase n-Butane," *International Journal of*

Thermophysics, vol. 22, p. 459–475, 2001.

[4] R. Span and W. Wagner, "Equations of State for Technical Applications. II. Results for Nonpolar Fluids," *International Journal of Thermophysics*, vol. 24, p. 41–109, 2003.

[5] B. A. Younglove and J. F. Ely, "Thermophysical Properties of Fluids. II. Methane, Ethane, Propane, Isobutane, and Normal Butane," *Journal of Physical and Chemical Reference Data*, vol. 16, no. 4, p. 577–798, 1987.

[6] T. Ito, Y. Nagata and H. Miyamoto, "Measurement of the (p, ρ, T) Properties for Pure Hydrocarbons at Temperatures up to 600K and Pressures up to 200 MPa," *International Journal of Thermophysics*, vol. 35, p. 1636–1646, 2014.

[7] I. M. Astina and H. Sato, "A Rational Helmholtz Fundamental Equation of State for Difluoromethane with an Intermolecular Potential Background," *International Journal of Thermophysics*, vol. 24, no. 4, p. 963–990, 2003.

[8] I. M. Astina, "Development of Fundamental Equations of State for Thermodynamic Properties of HFC Refrigerants," Ph.D. Dissertion, Keio University, Tokyo, 2003.

[9] S. Herrmann and E. Vogel , "Viscosity and Density of Normal Butane Simultaneously Measured at Temperatures from (298 to 448) K and at Pressures up to 30 MPa Incorporating the Near-Critical Region," *J. Chem. Eng. Data*, vol. 60, p. 3703−3720, 2015.

[10] H. Miyamoto and M. Uematsu, "The (p,v,T,x) Properties of (x1 Propane + x2 n-Butane) with x1 = (0.0000, 0.2729, 0.5021, and 0.7308) over the Temperature Range from (280 to 440) K at Pressures from (1 to 200) MPa," *J. Chem. Thermodynamics*, vol. 40, p. 240–247, 2008.

[11] S. Glos, R. Kleinrahm and W. Wagner , "Measurement of the (p, ρ, T) Relation of Propane, Propylene, n-Butane, and Isobutane in the Temperature Range from (95 to 340) K at Pressure up to 12 MPa Using an Accurate Two-sinker Densimeter," *J. Chem. Thermodyn.*, vol. 36, p. 1037–1059, 2004.

[12] H. Miyamoto and K. Watanabe, "A Thermodynamic Property Model for Fluid-Phase n-Butane,," *Int. J. Thermophys., 22(2),*, vol. 22, no. 2, p. 459–475, 2001.

[13] W. M. Haynes and R. D. Goodwin, "Thermophysical Properties of Normal Butane from 135 to 700 K at Pressures to 70 MPa," . NBS monograph 169, U.S. Department Commerce, , Washington, DC, 1982.

[14] P. J. Mohr , D. B. Newell and B. N. Taylor, "CODATA Recommended Values of the Fundamental Physical Constants," *Review of Modern Physics*, vol. 88, p. 1−73, 2016.

[15] I. M. Astina and H. Sato, "A Rapid Genetic Optimization Technique for Rational Thermodynamic Modeling Having Reliable Third Virial Coefficient," in *15th Symposium on Thermophysical Properties*, Boulder, 2003.

[16] K. Kan and I. M. Astina, "Effective Strategy of Modeling Helmholtz Equation of State," in *Proceeding The 10th AUN/SEED-Net Regional Conference on Mechanical and Manufacturing Engineeriing*, Phnom Penh, 2019.

[17] S. S. Chen, R. C. Wilhoit and B. I. Zwolinski, "Ideal Gas Thermodynamic Properties and Isomerization of n-Butane and Isobutane," , *J. Phys. Chem. Ref. Data*, vol. 4, p. 859–869, 1975.

[18] M. Jaeschke and P. Schley, "Ideal-Gas Thermodynamic Properties for Natural-Gas Applications," *Int. J. Thermophys*, vol. 16, no. (6), p. 1381−1392, 1995..

[19] Y. Kayukawa, M. Hasumoto, Y. Kano and K. Watanabe, "Liquid-Phase Thermodynamic Properties for Propane (1), n-Butane (2), and Isobutane (3)," *J. Chem. Eng. Data,*, vol. 50, p. 556−564, 2005..

[20] R. H. Olds, H. H. Reamer, H. H. Sage and W. N. Lacey, "Phase Equilibria in Hydrocarbon Systems, Volumetric Behavior of n-Butane," *Ind. Eng. Chem.*, vol. 36, no. 3, p. 82–284, 1944.

[21] W. M. Haynes, "Measurements of Densities and Dielectric Constants of Liquid Normal Butane from 140 to 300 K at Pressures to 35 MPa," *J. Chem. Thermodyn.*, vol. 15, no. 9, p. 801–805, 1983.

[22] D. Gupta and P. T. Eubank, "Density and Virial Coefficients of Gaseous Butane from 265 to 450 K at Pressures to 3.3 MPa," *J. Chem. Eng. Data*, vol. 42, no. 5, p. 961–970, 1997.

[23] W. B. Kay, "Pressure-Volume-Temperature Rerations for n-Butane," *Ind. Eng. Chem.*, vol. 32, no. 3, p. 358–360, 1940.

[24] J. E. Orrit and J. M. Laupretre, "Density of Liquefied Natural Gas Components," *Adv. Cryog. Eng.*, vol. 23, p. 573–579, 1978.

[25] W. M. Haynes and M. J. Hiza, "Measurements of the Orthobaric Liquid Densities of Methane, Ethane, Propane, Isobutane, and Butane," *J. Chem. Thermodyn.*, vol. 9, p. 179–187, 1977.

[26] C. R. McClune, "Measurement of the Densities of Liquefied Hydrocarbons from 93 to 173 K," *Cryogenics*, vol. 16, no. 5, p. 289–295, 1976.

[27] P. Sliwinski, "Die Lorentz-Lorenz-Funktion von Dampfförmigem und Flüssigem Äthan, Propan und Butan," *Z. Phys. Chem. Neue. Folge*, vol. 68, p. 263–279, 1969.

[28] J. W. Magee and T. O. D. Lüddeckke, "Molar Heat Capacity at Constant Volume of n-Butane at Temperatures from 141 to 342 K and at Pressures to 33 MPa," *Int. J. Thermophys.*, vol. 19, no. 1, p. 129–144, 1998.

[29] B. A. Younglove and J. F. Ely, "Thermophysical Properties of Fluids. II. Methane, Ethane, Propane, Isobutane, and Normal Butane," *J. Phys. Chem. Ref. Data*, vol. 16, p. 577−798, 1987.

[30] W. D. Machin and P. D. Golding, "Vapour Pressure of Butane from 173 to 280 K," *J.Chem. Soc.*, vol. 85, no. 8, p. 2229–2239, 1989.

[31] H. Holldorff and H. Knapp, "Vapour Pressures of n-Butane, Dimethyl Ether, Methyl Chloride, Methanol and the Vapor-Liquid Equilibrium of Dimethyl Ether-Methanol," *Fluid Phase Equilibria*, vol. 40, p. 113–125, 1988.

[32] H. Kratzke, E. Spillner and S. Müller, "Thermodynamic Properties for n-Butane, 1.The Vapour Pressure of Liquid n-Butane," *J. Chem. Thermodyn.*, vol. 14, p. 1175–1181, 1982.

[33] T. Sako, S. Horiguchi, H. Ichimaru and S. Nakagawa, "Vapour Pressure of Chlorine Trifluoride from 300 K to 317 K," *J. Chem. Eng. Data*, vol. 42, no. 1, p. 169–171, 1997.

[34] J. L. Flebbe, D. A. Barclay and D. B. Manley, "Vapor Pressures of Some C4 Hydrocarbons and Their Mixtures," *J. Chem. Eng. Data*, vol. 27, p. 405–412, 1982.

[35] B. P. Dailey and W. A. Felsing, "Heat Capacities of and Hindered Rotation in n-Butane and Isobutane," *J. Am. Chem. Soc.*, vol. 65, p. 44–46, 1943.

[36] M. B. Ewing, A. R. H. Goodwin, M. L. Mcglashan and J. P. M. Trusler, "Thermodynamic Properties of Alkanes from Speeds of Sound Determined Using a Spherical Resonator, 2. n-Butane," *J. Chem. Thermodyn.*, vol. 20, p. 243–256, 1988.

[37] A. E. Hawary and K. Meier, "Speed-of-Sound Measurements of Speed of Sound in Liquid n-Butane," *J. Chem. Eng. Data*, vol. 61, p. 3858–3867, 2016.

[38] R. Niepmann, "Thermodynamic Properties of Propane and n-Butane. 2. Speeds of Sound in the Liquid up to 60 MPa," *J. Chem. Thermodynamics*, vol. 16, p. 851–860, 1984.